Intense Beams of Polarized and Nearly Monochromatic Photons from Coherent Bremsstrahlung

R.T. Jones
University of Connecticut, Storrs, CT
and
Jefferson Lab, Newport News, VA

August 10, 1997

Abstract

One of the major considerations in planning photoproduction experiments is the choice of technique for generating the photon beam. Several possibilities exist, chiefly Compton-backscattered laser beams, tagged and untagged bremsstrahlung, and coherent bremsstrahlung from a crystal. In a coherent bremsstrahlung beam, collimation can be used to suppress the incoherent component and to narrow the energy spread of the coherent photon spectrum, producing beams with monochromatic peaks of only 1-2% r.m.s. width and high flux and polarization. The potential and limitations of this technique for use in photoproduction experiments at 8GeV and above are discussed in this report.

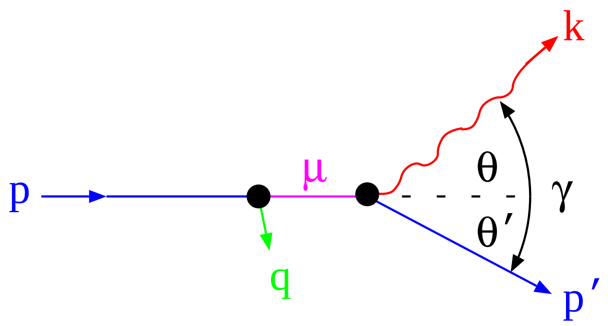

Figure 1: Kinematics of bremsstrahlung from an atom in the target, identifying the variables used in the text.

Coherent bremsstrahlung is common tehnique used in high energy physics to produce intense beams of highly polarized and monochromatic photons. In the literature, the term "coherent bremsstrahlung" is used to refer to two different effects. The first takes place when a highly relativistic electron is travelling inside a solid in a direction parallel to a crystal axis. In an effect known as *channeling*, the electron settles into a transverse well formed by chains of atomic nuclei, and enters the strong field regime in which higher-order QED processes dominate over Born terms in the production of bremsstrahlung. This appears experimentally as an enhancement over the normal bremsstrahlung spectrum at low photon energies, characteristic of multi-photon radiation. Theoretical models for this process employ a semi-classical picture for the radiation field, in which *coherent states* are used in the place of states with definite numbers of photons[1], hence the use of the term "coherent bremsstrahlung". In the more recent literature this is referred to as *channeling radiation*.

The second meaning for the term "coherent bremsstrahlung," which is the how it is used in this article, is the enhancement that occurs in normal bremsstrahlung inside a crystal when the momentum transfer from the electron to the atom matches a reciprocal lattice vector. This process, which is analagous to Bragg scattering, can be well described by first-order QED. The underlying cross section is the same as for Bethe-Heitler radiation, with the form factor augmented by additional factors for the crystal structure. The characteristics of the radiation pattern, however, are quite different from Bethe-Heitler (incoherent) bremsstrahlung, and these differences are what makes it interesting for our purposes. The reason is that for a given photon angle and energy, the incoherent spectrum is a sum over a continuum of momentum-transfer vectors, whereas in the coherent case the sum is discrete. This is best illustrated by a general description of the kinematics of bremsstrahlung.

1 Kinematics of bremsstrahlung

We are interested in the case where the electron is ultra-relativistic. The momentum transfer $\mathbf{q}$ to the atom is small compared to the atomic mass, so $q = (0, \mathbf{q}_T, q_l)$ and the energy transfer is negligible. The bulk of the cross section comes from momentum transfer values close to the peak of the function $|1 - F(q)|^2/q^2$ which corresponds to the atomic scale, around 10KeV. This allows one to keep only the leading terms in q/m_e. Momentum conservation at each vertex leads to the following relations.

$$\begin{aligned}
\mu^2 = (p-q)^2 &= (p)^2 + (q)^2 + 2\vec{p}\cdot\vec{q} &(1)\\
&= m_e^2 + 2pq_\ell + O(q^2) \\
\mu^2 = (p'+k)^2 &= (p')^2 + (k)^2 + 2E'k - 2\vec{p'}\cdot\vec{k} &(2)\\
&= m_e^2 + 2p'k\left(1 + \frac{m_e^2}{2p'^2} - \cos\gamma + O(\frac{m_e^4}{p'^4})\right) \\
2pq_\ell &= 2p'k\left(\frac{\gamma^2}{2} + \frac{m_e^2}{2p'^2}\right) + O(\gamma^4) &(3)
\end{aligned}$$

$$\gamma^2 \quad = \quad \frac{2pq_\ell}{p'k} - \frac{m_e^2}{p'^2} \tag{4}$$

The small-angle approximation is used because we are interested in forward angles within a few m_e/E radians. Apart from a small tranverse kick $\mathbf{q}_T$ (order 1μr for an 8GeV electron), the intermediate momentum vector points along the direction of $\mathbf{p}$. By contrast, the scattering angle at the second vertex scales as the electron mass (order 100μr for an 8GeV electron) so that one can consider the intermediate momentum to be along the incident beam axis and the transverse components of $\mathbf{k}$ and $\mathbf{p}'$ must balance each other. The initial-state radiation diagram looks somewhat different, but the kinematics are the same. These relations follow

$$\begin{aligned}
\gamma &= \theta + \theta' = \theta\left(1 + \frac{k}{p'}\right) = \theta\frac{p}{p'} \\
\theta^2 &= \left(\frac{1-x}{x}\right)\frac{2pq_\ell}{m_e^2} - 1
\end{aligned} \tag{5}$$

where x is the dimensionless photon energy (units of beam energy) and angles are measured in units of m_e/E. Eq. 5 is the desired result. From degrees-of-freedom counting it is clear that, once three-momentum conservation is used up constraining $\mathbf{p}'$ in terms of $\mathbf{k}$ and $\mathbf{q}$, there remains one more relation tying together $\mathbf{k}$ and $\mathbf{q}$; this is that relation, under the simplying approximations described above. It shows that for a given q_l there is a maximum photon energy, which is obtained at zero bremsstrahlung angle.

$$\max\left(x \equiv \frac{k}{p}\right) \quad = \quad \frac{2pq_\ell}{2pq_\ell + m_e^2} \tag{6}$$

Except for bremsstrahlung very near the end-point or at large angle, where the cross section is going to zero, the longitudinal component of $\mathbf{q}$ must be of order m_e^2/E, which is 32eV at 8GeV electron beam energy. The transverse component is not constrained by this condition and takes on values on the typical atomic scale of several KeV, leading to the conclusion that a momentum transfer $\mathbf{q}$ very nearly transverse to the incident direction is characteristic of bremsstrahlung scattering. The sum over all values of $\mathbf{q}$ which gives the incoherent bremsstrahlung spectrum of Bethe-Heitler leads to a distribution in bremsstrahlung angle which is independent of energy and forward-peaked with a characteristic opening angle of m_e/E, henceforth called 1. The integral over $\mathbf{q}$ conceals the angle-energy dispersion that is present at a particular value of $\mathbf{q}$, derived above from kinematics. This dispersion reappears in the case of coherent bremsstrahlung, where only a few discrete vectors contribute to the sum.

2 Coherent bremsstrahlung beams

By carefully adjusting the orientation of the crystal planes relative to the incident electron beam it is possible to make use of the crystal structure to greatly enhance the bremsstrahlung cross section at discrete values of $\mathbf{q}$ which correspond to the vectors of the reciprocal lattice. These enhancements show up as broad peaks superimposed upon the normal incoherent bremsstrahlung spectrum, with intensity comparable to or greater than the incoherent part. To obtain maximum enhancement, the crystal must be oriented so that one of its lowest-order lattice vectors falls within the range where the cross section is large, as described above. This means orienting the lattice so that the desired lattice vector is nearly perpendicular to the electron beam, with an inclination on the order of a few mr. By varying the crystal orientation, the peaks can be moved to provide the greatest photon flux at the energy of interest.

While it is not possible in general to orient the crystal so that only one lattice coherent peak appears in the photon spectrum, in a particular range of the photon spectrum there is generally one that is dominant. For individual values of $\mathbf{q}$ with x_{max} well below the end-point there is a high degree of polarization of the outgoing photon in the plane of $\mathbf{q}$ and the incident beam. By rotating the crystal with respect to the beam it is possible to orient in any transverse plane the polarization of the coherent component of the photon beam in the vicinity of an isolated coherent peak.

As discussed above, the hardest part of the coherent photon spectrum in any peak is kinematically confined to a cone much smaller than the characteristic bremsstrahlung angle m_e/E, making it possible to

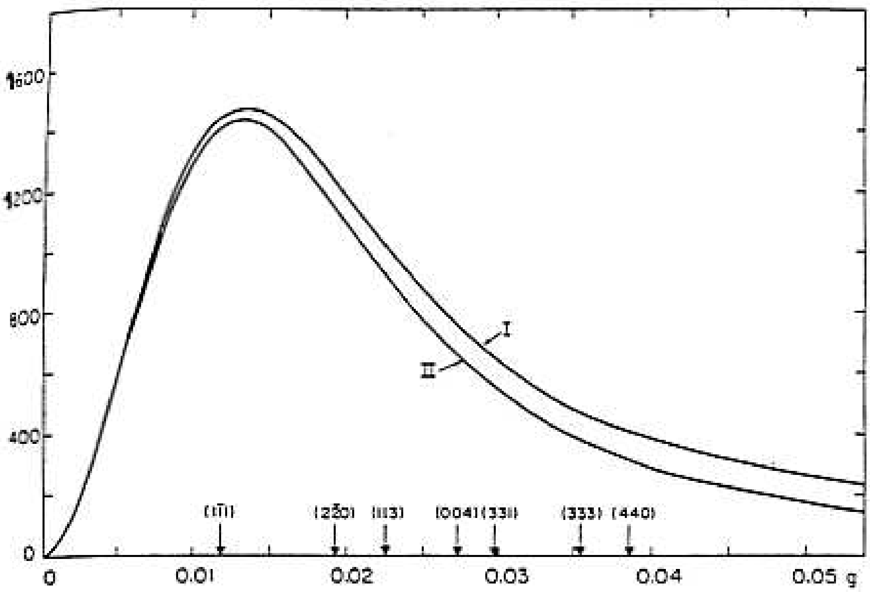

Figure 2: Curve I: $(1-F)^2/g^2$; curve II is curve 1 times $\exp(-Ag^2)$ *vs* g. This is Fig. 4 from Bilokon *et.al.*[3].

increase the relative intensity of the photon spectrum at the peak by collimation. Ideally such a technique would permit the generation of essentially monochromatic photon beams, with the low-energy bremsstrahlung background reduced to a negligible level. In this study I explore the potential of this technique for use as an alternative to tagged-bremsstrahlung or backscattered-Compton beams at CEBAF in the 8GeV+ era.

An example of an actual measurement made with such a beam at SLAC is described by Kaune *et.al.*[2]. Their paper also contains a compact description of the physics of coherent bremsstrahlung, and formed the starting point for this study.

3 Choice of crystal

The rate of coherent bremsstrahlung production be a high-energy electron in a crystal can be written in the following form.

$$\begin{aligned} \frac{dN_c}{dx\,d\phi} &= \frac{16\pi Z^2\alpha^3 p}{V^2 m_e^4} t \sum_i^{\text{planes}} \frac{g_{i\perp}^2}{g_i^4} \left|S(\vec{g}_i)\right|^2 \left|1-F(g_i^2)\right|^2 e^{-Ag_i^2} \\ & \quad \frac{1-x}{x^2(1+\theta^2)^4} \left((1+\theta^2)^2 \left[(1-x)^2+1\right] - 8\theta^2(1-x)\cos^2\phi\right) \\ S(\vec{g}) &= \sum_\nu^{\text{unit cell}} e^{i\vec{g}\cdot\vec{a}_\nu} \end{aligned} \tag{7}$$

The scattering angle is assumed to be an implicit function of $\mathbf{g}_i$ and x as given by Eq. 5. Consider the maximum of a given coherent peak, which occurs at x_{max} and $\theta = 0$. With crystal momentum $\mathbf{g}$ nearly transverse to the beam, the dependence on $\mathbf{g}_i$ enters through factors $|1-F(g)|^2/g^2$ and $\exp(-Ag_i^2)$. The first is the virtual photon flux factor. The second is the probability that a given photon can be absorbed or emitted by the crystal without absorbing or emitting additional phonons. The appearance of phonons in the process would introduce additional momenta to the problem, changing the kinematics and contributing to radiation that does not interfere with the phonon-free process. The following plot of these factors for carbon (diamond) is taken from Bilokon *et.al.*[3].

The upper [lower] curve excludes [includes] the exponential factor. The abscissa is shown in units of m_e. Markers are placed on the x axis to show the magnitudes of the lowest-order reciprocal lattice vectors.

In a same paper a survey of a lage number of single-element crystals was performed, and the value of the maximum in Fig. /refBilo4 calculated for each. It appears as column 7 in Table 1, also taken from the same reference.

The quantity M listed in last column of the table, which the authors call the *merit factor*, is simply column 7 multiplied by the number of lattice sites of the crystal per unit volume. The lesson drawn from this table is that only elements with the lowest Z are interesting as crystal radiators. Apart from a density factor t/AV, the merit factor collects together almost all of the crystal-dependence of the cross section. The one thing left over is the factor $(S/n)^2$ which has a maximum of 1. For a great many lattice vectors, symmetry in the unit cell gives rise to a cancellation that causes S to vanish. Therefore the relevant value of M is not the maximum, but rather the value at the lowest-order lattice vector for which S does not vanish. This the authors call the *performance parameter* P, tabulated in Table 2 for the most relevant crystals from Table 1, as a ratio of the performance parameter for diamond.

Considering its good mechanical properties and its availability as a high-quality crystal, diamond emerges the clear winner among the cases studied. The compound crystal Be_2C is somewhat superior in its performance, although little is known about how easy these crystals would be fabricate and to handle. The performance increment is probably not sufficiently great to stimulate much interest in their development.

4 Calculated spectra

As proof that the coherent bremsstrahlung spectrum can be adequately described by a first-order QED calculation such as the one described above, I show an experimental spectrum measured by a group at DESY using a 4.8GeV electron beam and a diamond crystal 1mm thick. The vertical axis is intensity, a dimensionless quantity $I = xdN/dx$ in which the incoherent cross section is approximately flat. The solid dots are the measurements. The dashed curve is the calculated ideal spectrum for a thin crystal, and the solid curve is the calculation including multiple-scattering and beam divergence effects. The dot-dashed curve is the incoherent contribution alone. The agreement with the solid curve supports the claim that experimental spectra, including the defects present in a real beam and target, can be reliably calculated within the simple framework described in this report.

The crystal structure of diamond is shown in Fig. 4. Consider first an incident electron beam directed along $\mathbf{a}_1$. The only reciprocal lattice vectors with small projections onto $\mathbf{a}_1$ would be those lying in the plane (0,1,0), (0,0,1). Ideally these would have vanishing projections onto the beam axis, but finite emittance and imperfect crystal alignment cause a certain spread in q_l about zero. Since low q_l means low x, this leads to enhanced bremsstrahlung production at the low end of the photon spectrum, such as appears in Fig. 3. To raise the energy of the coherent peak, one can tilt the crystal by a small angle about one of the symmetry axes perpendicular to the beam; either (0,1,1) or (0,-1,1). After this rotation only a few rows of lattice vectors contribute significantly to the sum, instead of a whole plane, with each row showing up as a discrete peak (see Fig. 3). There is still the problem, however, that there is a single row passing through the origin in q-space and parallel to the rotation axis. The lattice vectors in this row all have a vanishing projection onto the beam axis, and through beam divergence *etc.* give rise to a very large coherent peak at zero photon energy with a tail extending under the other coherent peaks. Note that in the above spectrum the vertical axis is Intensity, not photon flux, so that the normal bremsstrahlung spectrum is approximately flat (see dot-dashed line). The user of a bremsstrahlung photon beam would generally be ill- prepared to accept such a large surplus of background photons over what is already present in a conventional bremsstrahlung beam. The authors of the paper from which Fig. 3 was taken were able to reproduce this peak in their calculation, and identify its cause. They cut it off in their plot, otherwise it would suppress the scale.

The production of a coherent low energy peak can be eliminated completely by tilting around both axes (0,1,1) and (0,-1,1) simultaneously. The first tilt is by a large enough angle that all of the peaks in Fig. 3 are pushed up to $x = 1$ (where they disappear, leaving only the peak at zero) and then the second tilt is tuned to move the zero-peak up to the desired energy. The zero-peak turns out to be a whole sequence of peaks, but the lowest-energy one is the strongest. It is not possible to select only one lattice vector, and so obtain only one peak in the spectrum, but the remaining peaks are nicely separated from one another in energy and so do not really cause problems to the user of the coherent photon beam. One side effect of this dual-rotation procedure is that, by narrowing to just one the number of lattice vectors contributing

Table 1: Merit factor of selected crystals; taken from Bilokon *et.al.*[3] Table 1.

Element	Z	Structure type [a)]	n	Lattice constants (Å&deg.)	$\check{V}$ (Å)^3	$(1-F)^2/g^2$ (MAX)	$\check{M}$
Li	3	b.c.c.	2	3.51	43.2	2727	126
Be	4	h.c.p.	2	2.29; 3.58	16.3	2667	326
Be α	5	rhomb.	12	5.06; 58.10^o	87.4	2124	292
C (diamond)	6	diam.	8	3.57	45.5	1462	257
C (graphite)	6	hexagonal	4	2.46; 6.71	35.2	1462	166
Na	11	b.c.c.	2	4.29	79.0	625	16
Mg	12	h.c.p.	2	3.21; 5.21	46.5	761	33
Al	13	f.c.c.	4	4.05	66.4	882	53
Si	14	diam.	8	5.43	160.1	936	47
Ti	22	h.c.p.	2	2.95; 4.69	35.3	724	41
Fe α	26	b.c.c.	2	2.87	23.6	563	48
Co α	27	h.c.p.	2	2.51; 4.07	22.2	529	48
Ni	28	f.c.c.	4	3.52	43.6	498	46
Cu	29	f.c.c.	4	3.62	47.4	464	39
Zn	30	h.c.p.	2	2.66; 4.93	30.2	443	29
Ge	32	diam.	8	5.66	181.3	424	19
Mo	42	f.c.c.	4	4.16	72.0	470	26
Rh	45	f.c.c.	4	3.80	54.9	453	33
Ag	47	f.c.c.	4	4.09	68.4	436	25
Sn α	50	diam.	8	6.49	273.4	418	12
Ta	73	b.c.c.	2	3.31	36.3	289	16
W	74	b.c.c.	2	3.17	31.9	288	18
Ir	77	f.c.c.	4	3.84	56.6	287	20
Pt	78	f.c.c.	4	3.92	60.2	287	19
Au	79	f.c.c.	4	4.08	67.9	287	17
Tl α	81	h.c.p.	2	3.45; 5.51	56.8	285	10
Pb	82	f.c.c.	4	4.95	121.3	284	9
Be_2B	4,5	CaF_2	12	4.66	101.2	2667	316
Be_2C	4,6	CaF_2	12	4.34	81.7	2667	392
B_4C	5,6	rhomb.	15	5.17; 65.5^o	112.0	2124	284

[a)] f.c.c. = face centered cubic; b.c.c. = base centered cubic; h.c.p. = hexagonal closest packing; diam. = diamond; rhomb. = rhombohedral; CaF_2 = CaF_2 cubic type.

Table 2: Performance parameter P relative to that of diamond; taken from Table 2 of Bilokon *et.al.*[3]

Crystal	Best reciprocal vector	P/P_{diamond}
Diamond	$2\bar{2}0$	1.00
Beryllium	002	0.86
Boron	208	0.38
Silicon	$2\bar{2}0$	0.19
Be_2C	220	1.10

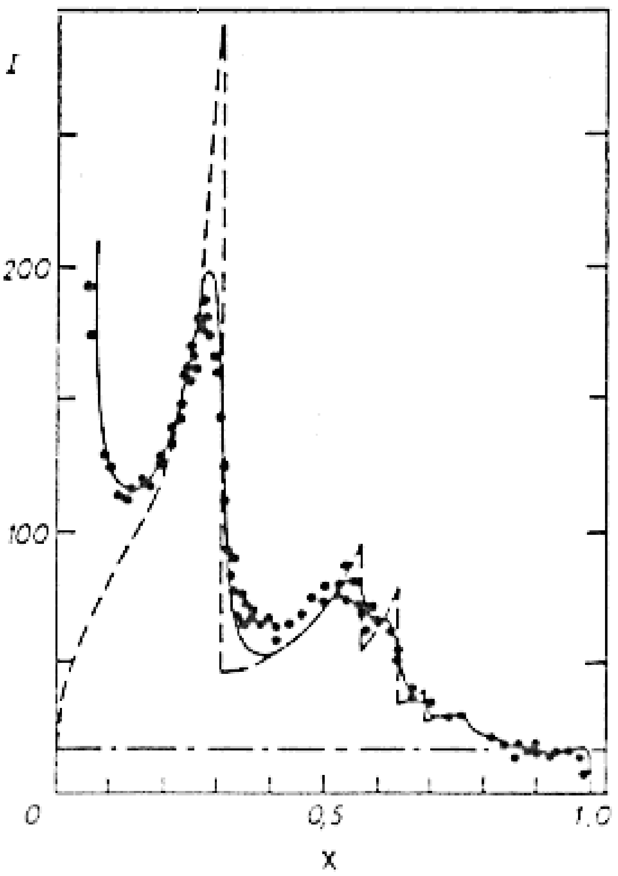

Figure 3: Bremsstrahlung intensity *vs.* $x = k/E_0$ for diamond, $E_0 = 4.8$GeV; $\theta < 3.44$mr. This is Fig. 2 from Bilokon *et.al.*[3].

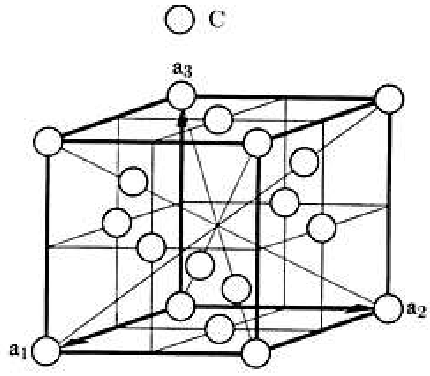

Figure 4: Crystal structure of diamond.

to a peak, the photons within a peak are very highly polarized in the plane containing the lattice vector and the beam. A drawback of the dual-rotation procedure is that the coherent enhancement is less when a single lattice vector contributes than when a whole row of vectors contribute, a factor of 3 for diamond on the (0,2,2) vector. I take the point of view that a clean beam is more important than raw photon flux per electron.

Using the above prodecure to fix the crystal orientation, I show below the total bremsstrahlung spectrum for a 8GeV electron beam. The angles were adjusted for peak photon flux at half the end-point. By plotting the total bremsstrahlung over incoherent, the degree of coherent enhancement is made clear. The wiggles in the vicinity of the sharp edges are smoothing artefacts of the plotting package. Note that the spectrum drops to unity (no coherent component) at the infrared limit.

Actually the distinction between coherent and incoherent components is somewhat artificial in these calculations. The incoherent radiation is *not* the same as that from an amorphous radiator of the same thickness. When one replaces the integral over $\mathbf{q}$ with a discrete sum, the sum is only carried out for relatively small integers (h, k, l), beyond which the terms are squelched by the phonon decoherence factor $\exp(-Aq^2)$. Beyond that the crystal structure is irrelevant and the atoms contribute individually. The large-q part of the sum in these calculations is replaced by an integral, as for Bethe-Heitler, but here the integral must exclude the piece covered by the discrete sum in order to prevent double-counting. This large-q part, which has the same spectrum as ordinary bremmstrahlung, is called the incoherent component in these calculations. For diamond, this incoherent part is 15% less than would be obtained with an amorphous carbon radiator of the same thickness in g/cm^2.

As discussed in the section above on kinematics, there is a tight correlation within the coherent peaks between the bremsstrahlung energy and angle of emission with respect to the incident electron direction. By collimating the photon beam, one can eliminate photons beyond a certain angle, and narrow the width of the peaks in energy. In Figs. 6-8 is shown the effects of progressively collimating the photon beam to smaller and smaller angles. Plotting the spectra in this way displays in a clear way how collimation narrows the peaks and increases the coherent fraction of the beam. The polarization of the coherent component in these peaks is greater than 80%. The blue-shaded region of Fig. 9 gives the relative number of polarized photons. Outside the coherent peaks the polarization is zero.

5 Limiting effects

It would appear from the above sequence that one could in this way produce a photon beam of arbitrarily good energy resolution (within a given peak) and low background. Actually there are limits on how far this procedure can be taken. These limits are described in this section.

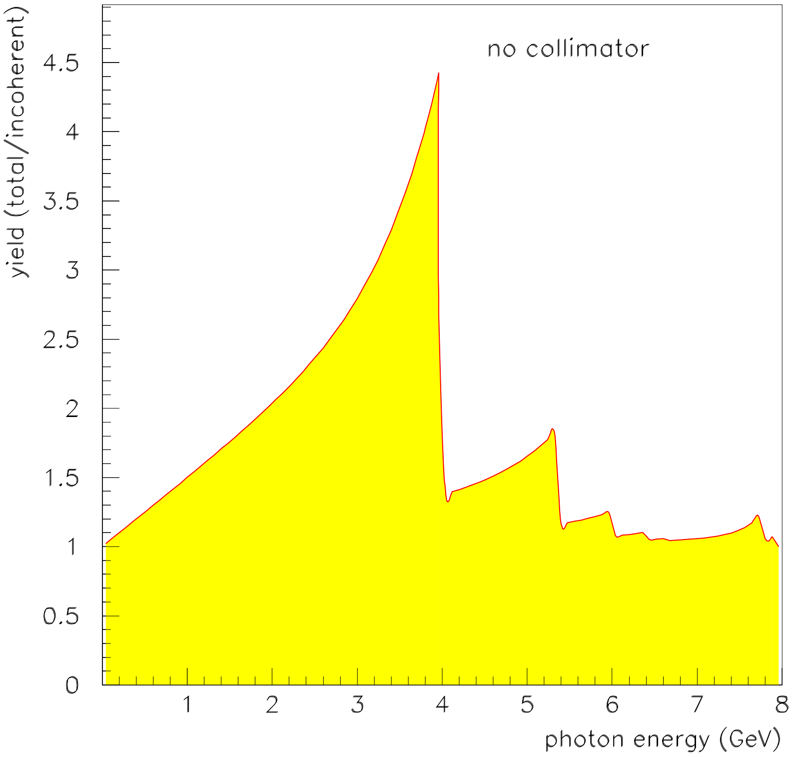

Figure 5: Uncollimated coherent bremsstrahlung spectrum, plotted *vs.* photon energy in units of the incoherent flux. The calculation assumes an electron beam of 8GeV incident on a diamond crystal oriented to place the strongest coherent peak at 4GeV.

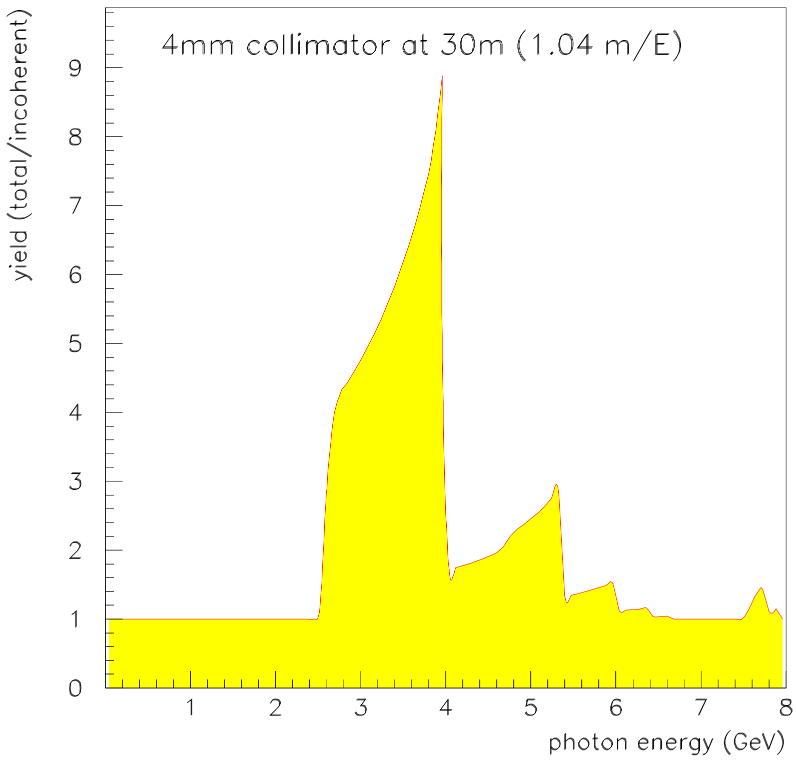

Figure 6: Same spectrum as shown in Fig. 5 but including only photons generated within $1.04 m_e/E$ of the incident electron direction.

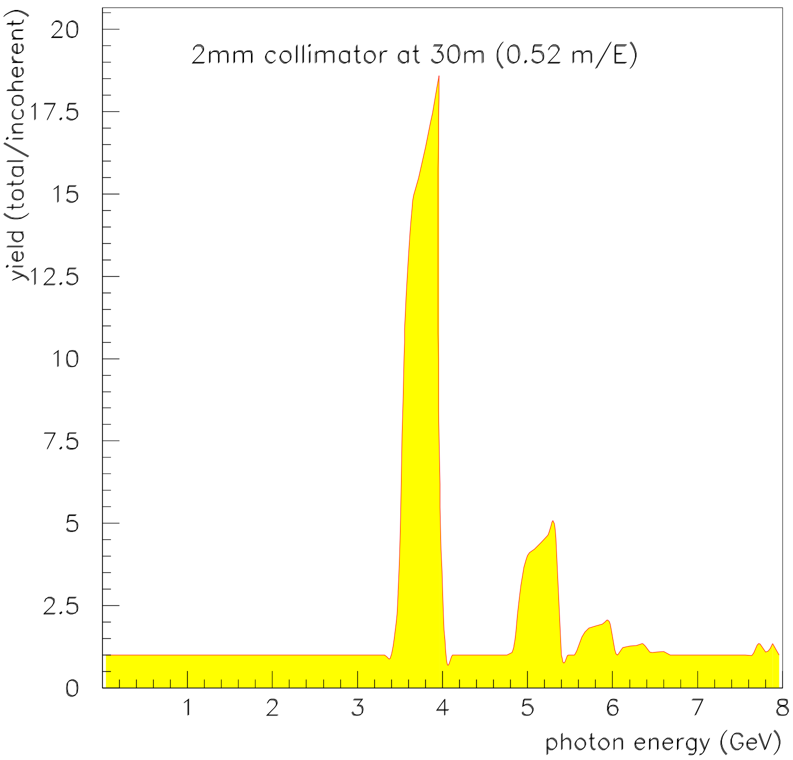

Figure 7: Same spectrum as shown in Fig. 5 but including only photons generated within $0.52 m_e/E$ of the incident electron direction.

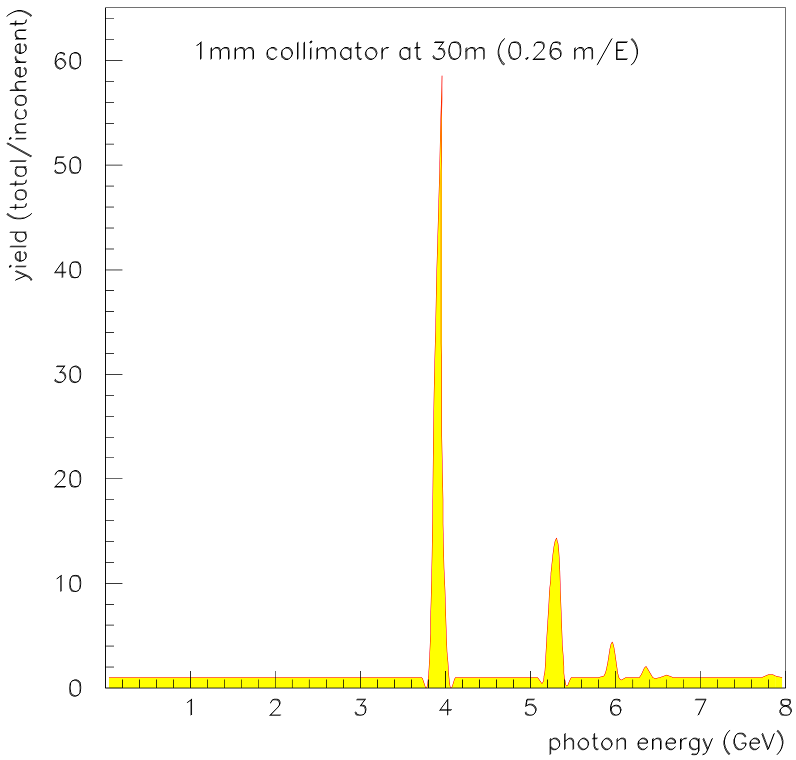

Figure 8: Same spectrum as shown in Fig. 5 but including only photons generated within $0.26m_e/E$ of the incident electron direction.

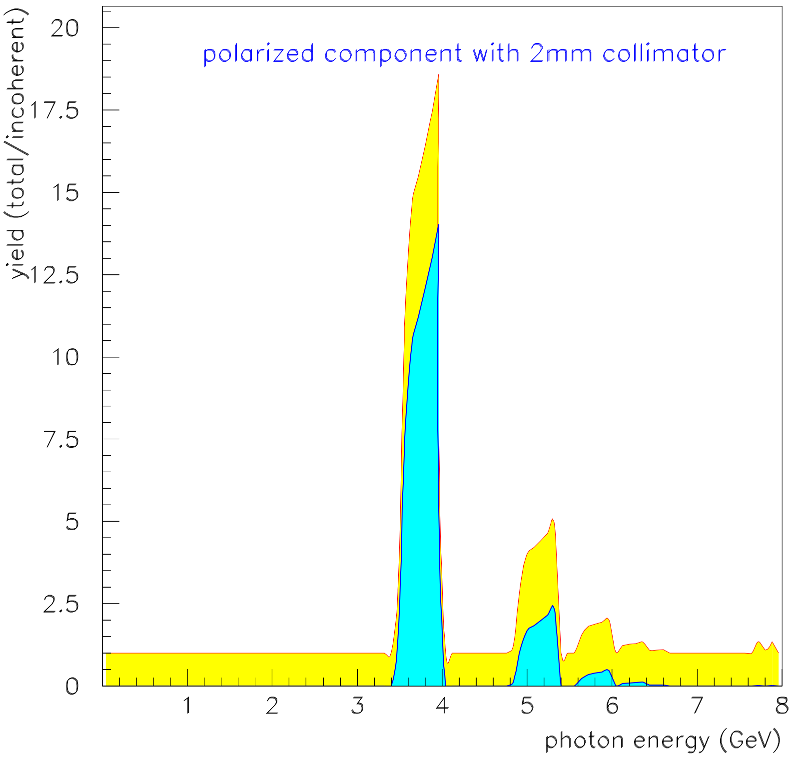

Figure 9: Same spectrum as shown in Fig. 7 (shaded in yellow) with the polarized flux superimposed (shaded in blue). The plane of polarization can be rotated simply by a rotation of the crystal about the beam axis.

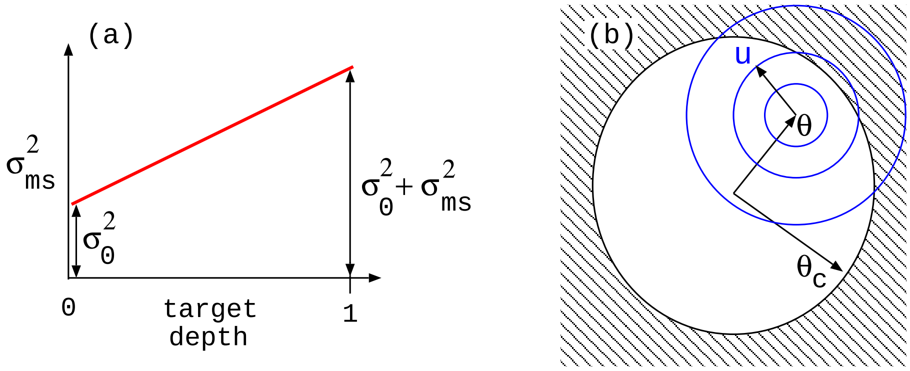

Figure 10: Depiction of the effects of electron multiple-scattering in the target on the effectiveness of photon beam collimation. At the left (a) is shown the mean-squared divergence of the electron beam as a function of depth inside the target, showing the linear dependence of multiple scattering on target thickness. At the right (b) is shown the collimator plane and the three principal angles used in the text: the angle θ_C subtended by the collimator boundary from the center of the radiator, the bremsstrahlung emission angle θ with respect to the electron direction, and the angle of divergence u of the electron with respect to the nominal beam direction, at the instant of radiation. The blue circles represent a contour map of the photon beam in angle space for a given bremsstrahlung angle.

5.1 multiple scattering

The lower edge on the coherent peaks in Figs. 5-8 appear because all photons beyond a certain bremsstrahlung angle were absorbed by the collimator. A collimator does not actually cut in bremsstrahlung angle, but rather the angle between the photon and the *nominal* electron beam axis. Any divergence of the radiating electron from its nominal direction would smear out the cut in bremsstrahlung angle, and broaden the edge in the energy spectrum. The most important source of beam divergence is the multiple scattering that takes place inside the radiator itself before the coherent photon is produced. Since for thin radiators the radiation probability is roughly uniform throughout the crystal, the effective beam distribution is an average over radiation depth.

$$
\begin{aligned}
p(\theta) &= \int_0^1 dt \frac{\exp\left(-\frac{1}{2}\frac{\theta^2}{\sigma_0^2+t\sigma_{ms}^2}\right)}{2\left(\sigma_0^2+t\sigma_{ms}^2\right)} \\
&= \frac{1}{2\sigma_{ms}^2}\left[\mathrm{Ei}\left(\frac{\theta^2}{2(\sigma_0^2+\sigma_{ms}^2)}\right)-\mathrm{Ei}\left(\frac{\theta^2}{2\sigma_0^2}\right)\right]
\end{aligned}
\tag{8}
$$

The probability density $p(u)$ differential in du^2 represents the dispersion of impacts on the collimator plane from photons generated at fixed bremsstrahlung angle, as illustrated in Fig. 10b. Including the effects of multiple scattering, instead of a rectangular function in bremsstrahlung angle with a sharp cutoff at the collimator diameter, the collimation is described by an acceptance function which varies smoothly from a maximum at the origin to zero for angles far outside the collimator. More specifically, the acceptance function is the two-dimensional integral of $p(u)du^2$ over the surface excluded by the hatched zone shown in Fig. 10b.

This function is calculated by numerical integration. It is plotted in Fig. 11 for three different thicknesses of diamond radiator, using a collimator of nominal radius 0.5 m_e/E. Note that at 100μm thickness, the acceptance never rises above 50%, even at 0^o, due to multiple scattering. The effects of multiple scattering become more pronounced the more narrow is the collimation. For the 0.25 m_e/E collimator the shape of the energy peak is dominated by multiple scattering, even for the very thin radiator thickness of 10μm. This is shown in Fig. 12. The colour codes have the same meaning as in Fig. 11.

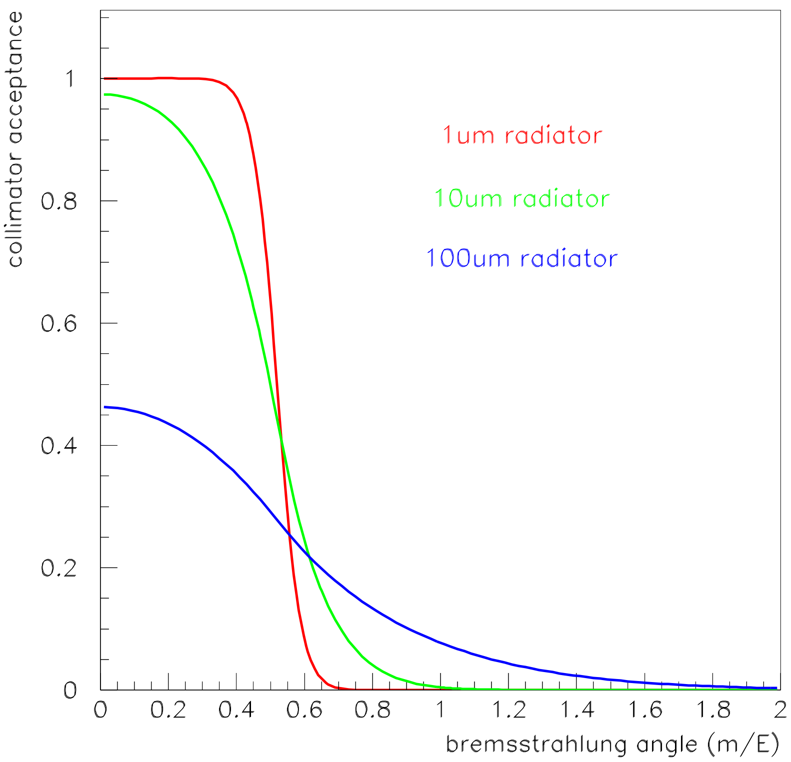

Figure 11: The acceptance function for collimation at $0.52\, m_e/E$ for various thicknesses of diamond radiator, after taking into account multiple scattering of the electron inside the crystal.

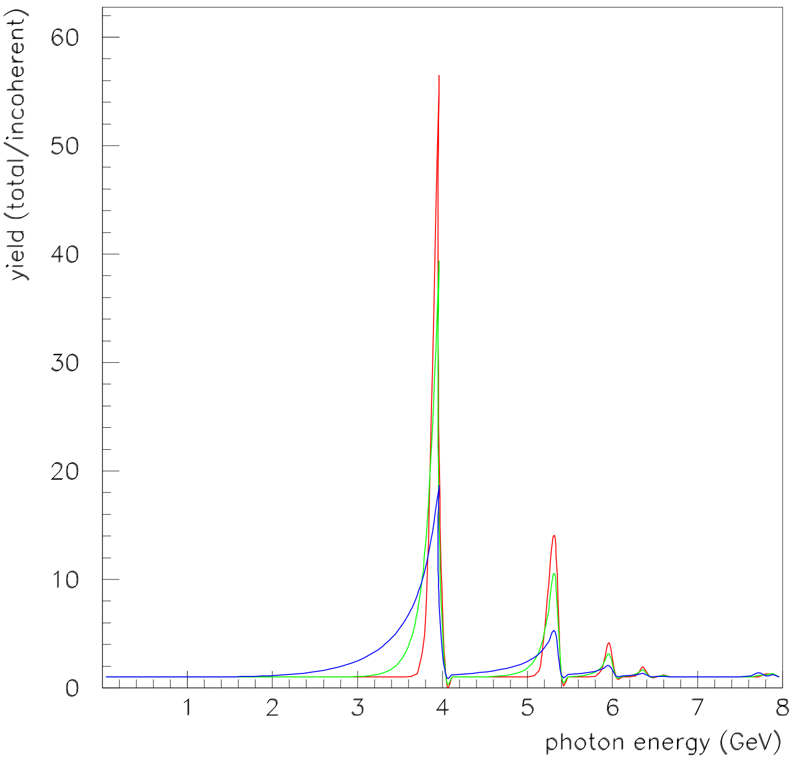

Figure 12: Modifications to Fig. 8 after taking into account multiple-scattering inside the target, for three choices for the thickness of the radiator. The colour codes are the same as those used in Fig. 11.

5.2 beam spot size

In the preceding section, the beam was asummed to zero emittance at the entrance to the radiator, in order to isolate the effects of multiple scattering on the energy spectrum of the beam. When finite electron beam emittance effects are included, the above picture is modified in two ways. First, the electron beam has an intrinsic spread in addition to that arising from multiple scattering. This was anticipated in the previous section with the incorporation of the σ_0 parameter, which up to now has been set to zero. Second, for a given crystal orientation, the projection of $\mathbf{q}$ onto the incident momentum axis is slightly different for each particle in the beam, with the effect that the curve relating bremsstrahlung angle to energy x broadens into a band. In summary, the second effect smears out the map from energy to bremsstrahlung angle, while the first smears out the map from bremsstrahlung angle to position on the collimator plane. Discussion of the second effect is postponed to the next section.

Taking into account the effects of beam emittance on the collimator-plane angular resolution amounts to evaluating the constant σ_0 from a given beam specification. Referring to the picture in Fig. 10b of photon impact on the collimator plane, consider the following for a very thin radiator so that multiple scattering can be neglected. In the limit of negligible angular divergence of the beam, the distribution $p(u)$ of hits on the collimator plane will be essentially the image of the beam spot. If the beam is focused to a negligible spot at the radiator position then this distribution will be the momentum-space image of the beam in the plane transverse to the nominal incident direction. A realistic situation falls somewhere in between, so that σ_0 depends in some way both on coordinate-space and momentum-space r.m.s. widths of the beam at the radiator. The picture is much simpler if one considers the virtual image of the beam at the position of the collimator. The image is virtual because the real electron beam is broadened by multiple scattering and bent into the dump, so it looks quite different at the collimator plane. The virtual image is formed by free-motion transport of the electron beam phase-space distribution, as it is at the entrance to the radiator, downstream to the entrance plane of the collimator. Considered there, $p(u)$ is simply the coordinate-space image of the beam in the transverse plane, converted to radians by dividing by the radiator-collimator distance.

The product of coordinate-space and momentum-space r.m.s. widths of the beam, called *emittance*, is a fixed property of the accelerator. It is only modified by radiation or interactions of the beam with matter, and not by passive beamline elements. For this study the emittance is taken to be $4 \cdot 10^{-9}$rm, which I believe to be a conservative figure for CEBAF. With the emittance fixed, we are free to adjust the beam optics to project the desired spot size at the collimator. A lower limit on the spot size is given by the distance to the focusing elements, where the beam must be correspondingly large in order to focus down to the desired spot size, and yet small enough to avoid aberrations from to higher-order field components. If the quads-to-collimator distance is 40m and the beam is limited to 2mm r.m.s. at the quads, this gives a minimum spot size around 100μm at the collimator. As will be seen from the next section, the divergence properties of such a strongly focused beam has other effects on the coherent bremsstrahlung beam, which favour relaxing the spot size requirement somewhat. In Fig. 13 is shown the trend in collimation resolution as the spot size is adjusted within what I consider to be reasonable limits.

Note that the spot size sets an effective lower limit on the distance from radiator to collimator. Simply reducing this distance by some factor in combination with a similar reduction in collimator diameter does not produce a beam of the same quality. This is because the beam spot sets a length scale for the smearing of the collimator cutoff which does not scale with the distance to the radiator, for a given beam optics. In general one should ensure that the radiator-collimator separation is sufficient that the smallest collimators of interest are much larger than the virtual beam spot size. In Fig. 14 is plotted the photon beam profiles corresponding to the three choices of beam spot size in Fig. 13. For these studies the effects of multiple scattering were suppressed in order to accent the effects of beam emittance.

5.3 beam divergence and crystal mosaic spread

As mentioned in the previous section, there are two separated ways in which finite beam emittance modifies the naive picture of ideal collimated bremsstrahlung. The first, described above, contributes along with multiple scattering in smearing out the relation between bremsstrahlung angle and impact on the face of the collimator. Given unlimited real estate and possibilities for special optics, this problem can be reduced arbitrarily by reducing the size of the virtual beam spot at the entrance to the collimator. Owing to the irreducibility of the beam emittance, this reduction carries with it an increase in the divergence of the beam

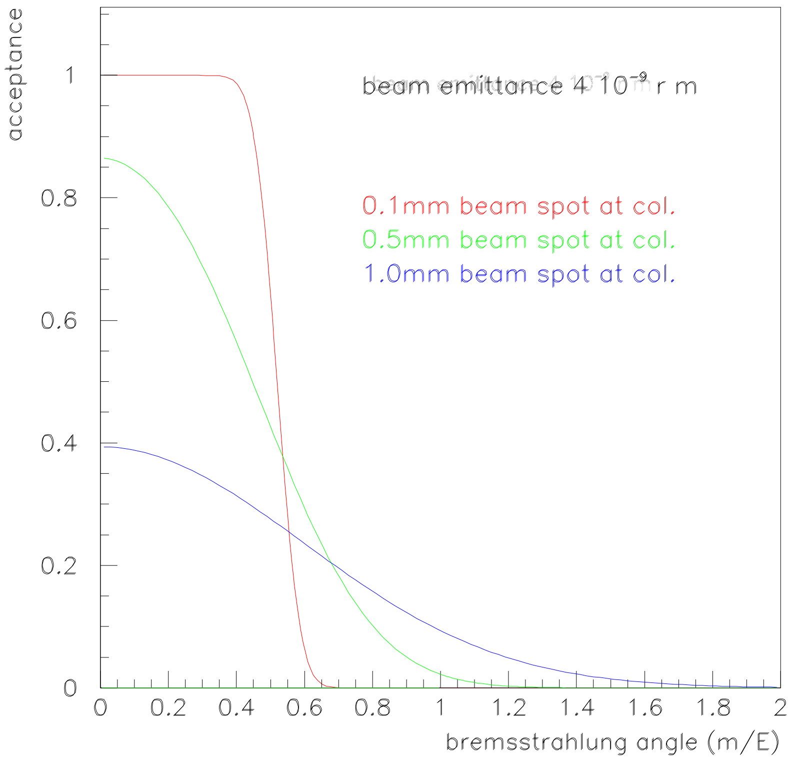

Figure 13: Collimator acceptance function with a 0.52 m_e/E collimator for various virtual electron beam spot sizes at the plane of the collimator.

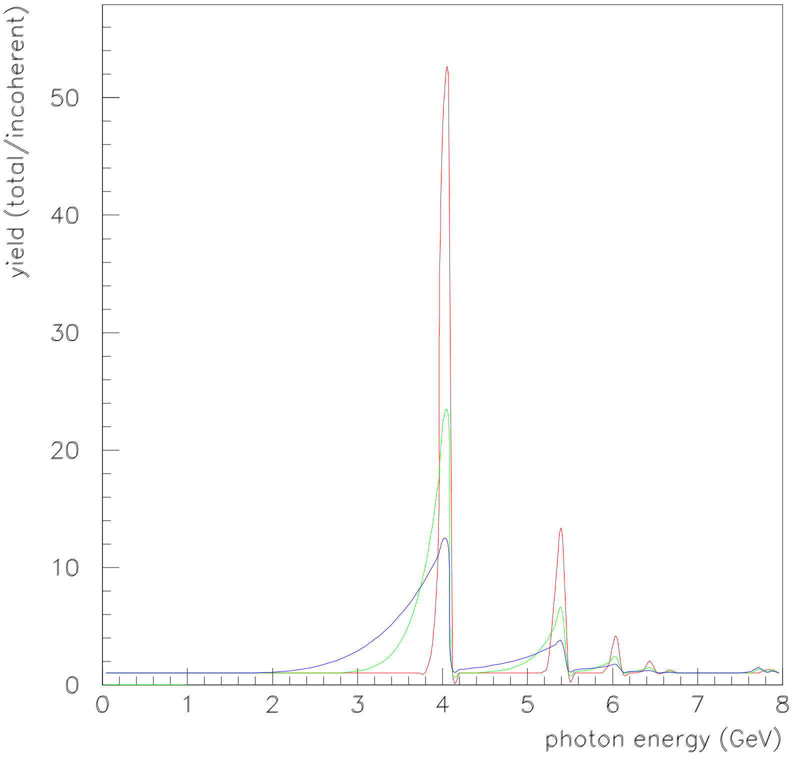

Figure 14: Modifications to Fig. 8 after taking into account the effects of finite electron beam spot size as projected from the radiator onto the plane of the collimator. The colour codes are the same as those used in Fig. 13.

at the radiator which has another effect, that of smearing out the exact relation which exists ideally between bremsstrahlung angle and energy for the coherent component of the beam.

This smearing takes place because each electron in the beam has a slightly different incidence angle to a given crystal plane, and hence a different value of q_l which relates x to angle (see Eq. 5). Small non-planarities of the crystal also contribute to this smearing, an effect known in crystalography as *mosaic spread.* Multiple scattering also makes a contribution. To lowest order, a shift in q_l with no change in the angular acceptance results in a shift of the peak in x.

$$x = \frac{2pq_\ell}{2pq_\ell + (1+\theta^2)m_e^2} \tag{9}$$

$$\delta x \mid_{\text{const }\theta} = x(1-x)\frac{\delta q_\ell}{q_\ell} \tag{10}$$

Following the same treatment as outlined above under multiple scattering, the mean-square beam divergence enters the crystal with a value σ_0^2 and exits with $\sigma_0^2 + \sigma_{ms}^2$. This angular spread translates into a smearing in x given by the function $f(x, x')$

$$\begin{aligned} f(x,x') &= \frac{1}{\sqrt{2\pi}}\int_0^1 dt\,\frac{\exp(-\frac{\alpha^2(x-x')^2}{2x'^2(1-x')^2(\sigma_0^2+t\sigma_{ms}^2)})}{\sqrt{\sigma_0^2+t\sigma_{ms}^2}} \qquad (11)\\ &= \sqrt{\frac{2}{\pi}}\frac{1}{\sigma_{ms}^2}\left[\sqrt{\sigma_0^2+\sigma_{ms}^2}\exp\left(-\frac{\alpha^2(x-x')^2}{2x'^2(1-x')^2(\sigma_0^2+\sigma_{ms}^2)}\right)\right.\\ &\qquad\left. - \sqrt{\sigma_0^2}\exp\left(-\frac{\alpha^2(x-x')^2}{2x'^2(1-x')^2\sigma_0^2}\right)\right]\\ &\quad+\frac{\alpha(x-x')}{x'(1-x')\sigma_{ms}^2}\left[\mathrm{Erf}\left(\frac{\alpha(x-x')}{x'(1-x')\sqrt{2(\sigma_0^2+\sigma_{ms}^2)}}\right)\right.\\ &\qquad\left. - \mathrm{Erf}\left(\frac{\alpha(x-x')}{x'(1-x')\sqrt{2\sigma_0^2}}\right)\right] \\ \text{where}\quad \alpha &\equiv \frac{q_\ell}{|\vec{q}|}\end{aligned}$$

which is applied to the x-distribution as the last step in the calculation described in this report.

$$\left(\frac{dN}{dx}\right)_{\text{corr}} = \int_0^1 dx'\,f(x,x')\frac{dN}{dx'} \tag{12}$$

This smearing conserves the integral of counts in the spectrum, and has the effect of smoothing out the sharp edges of the peaks. To isolate the effects of crystal quality, I suppress beam emittance and multiple scattering in Fig. 15, and explore a range of values for mosaic spread.

The energy scale is expanded in Fig. 15 to highlight the differences between the curves. A diamond crystal with mosaic spread below $100\mu r$ is considered to be "almost perfect" by Bilokon *et.al.*[3]. If this is the case then for electron beams available at CEBAF, the mosaic spread dominates over beam emittance and multiple scattering in determining the degree of energy/angle smearing. In an experimental spectrum it is possible to read the mosaic spread directly from the sharpness of the high-energy edge of the coherent peak.

5.4 radiation damage to crystal

From the foregoing considerations, it is clear that multiple scattering is the most important limitation to the resolution that can be obtained by severe collimation of coherent bremsstrahlung. To control multiple scattering one would like to decrease the target thickness, and make up the flux by increasing the electron beam current. Besides the technical difficulty of fabricating and positioning very thin crystals, there are two effects which place lower bounds on target thickness. The first arises from the need for a sufficient number

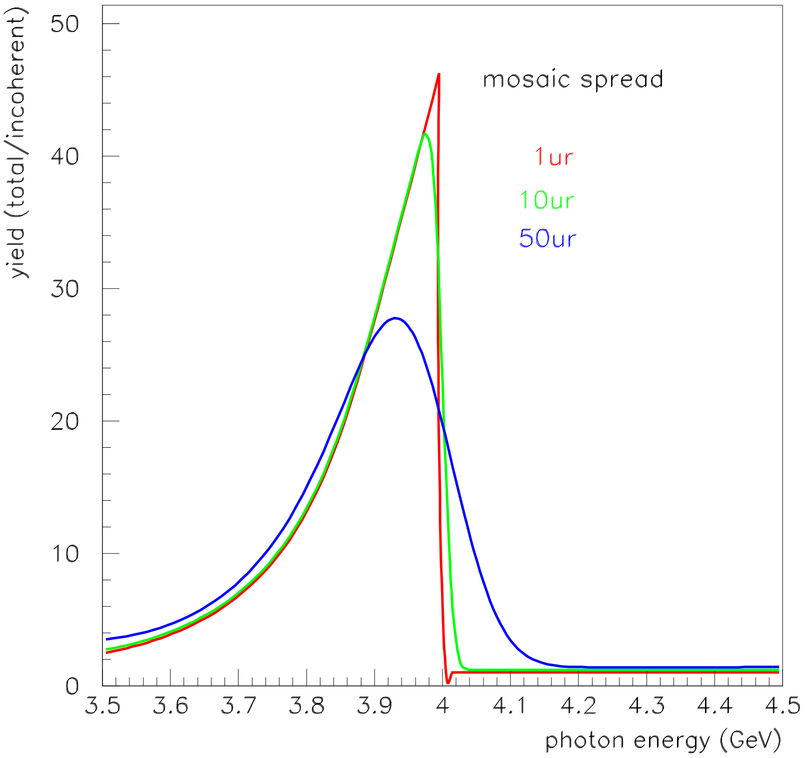

Figure 15: Modifications to Fig. 8 after taking into account the effects of crystal quality, for different values of the average mosaic spread. Note that the horizontal scale has been expanded relative to Fig. 8

of atomic layers to provide interference which gives rise to coherent enhancement. This bound is simply the longitudinal coherence length of the virtual photon, $1/q_l$ in units where $\hbar = c = 1$. For the energies of interest here, this is of order 10^{-8}m, far from the regime of practical concern.

The second effect which limits the use of thin radiators is the radiation damage suffered by the crystal during exposure to high currents. Kaune *et.al.*[2] report that at SLAC they found it necessary the remove the diamond and treat it with an anealing process after it had seen $2 \cdot 10^{19}$ electrons. The beam spot had a diameter of roughly 6mm at the radiator, which leads to a radiator lifetime of $7 \cdot 10^{19} e^-/\mathrm{cm}^2$ for the SLAC 80μm diamond. Bilokon *et.al.*[3] estimate $10^{20} e^-/\mathrm{cm}^2$ for diamonds several mm thick. Others have estimated longer lifetimes by a factor of 2-3. In this report I take $10^{20} e^-/\mathrm{cm}^2$ to be a conservative estimate.

In order to translate this into duration for an experiment, I need to make some assumptions about the experimental rate requirements. For this study I take the design parameters that were used for the current RadPhi (E94-16) experiment. Detector and trigger were designed assuming a tagged bremmstrahlung beam of 4GeV end-point, with a total tagging rate of $5 \cdot 10^7$ photons/s in the energy range [3.0,3.8]GeV. I I furthermore assume that this represents a limit for rates in the detector elements, so that one would not run with higher currents even if tagging accidentals were not a problem. Since most of the rate in the detectors comes from the untagged flux at low energies, a coherent radiator could enhance the rate of good triggers without appreciably affecting the overall rates in the detectors. Under these conditions and without any collimation, the rate within the interval [3.0,3.8]GeV could be increased from $5 \cdot 10^7$ to $17 \cdot 10^7$ photons/s. Of course without collimation the coherent energy peaks are very broad, and use of the tagger would be required, limiting the usable rates to a few 10^7. In the absense of collimation, there is no reason to use ultra-thin crystals, and thicknesses up to 1mm are basically equivalent. The lifetime of the radiator under these circumstances is on the order of years, much longer than the duration of an experiment.

To bypass the flux limitations of tagging, one must give up the energy information from the tagger. Depending on the requirements of the experiment, the narrow peaks from collimated coherent bremsstrahlung may provide sufficient resolution for the data analysis. The primary use of the tagger information in RadPhi is to limit the online trigger rate by rejecting events from untagged flux. At a tagging rate of $5 \cdot 10^7$ and a coincidence window of 15ns the rejection power has dropped to 50%. At this point one might eliminate tagging in favour of collimated coherent bremsstrahlung. One could drop the incoherent bremsstrahlung flux by a factor of two to maintain the same low-level trigger rates, and still enhance the rate of good triggers by a considerable fraction.

I consider two cases: a 100μm radiator (thick) and a 10μm radiator (thin). In the case of the thick radiator, the multiple scattering limits useful collimation to roughly 0.5 m_e/E, or 2mm at 30m. The r.m.s. width of the peak is 10%, covering fully the original tagging range [3.0,3.8]GeV. The photon flux in this window is $2.2 \cdot 10^8$, a factor of 4 increase. The spectrum is shown by the blue curve in Fig. 16. In the case of the thin radiator, the collimation is reduced to 0.25 m_e/E, or 1mm at 30m. The r.m.s. width of the peak is 4%, centered at 3.6GeV. The total photon flux is $2.7 \cdot 10^8$ within the interval [3.0,3.8]GeV, an increase by a factor greater than 5. The spectrum is shown by the red curve in Fig. 16.

The beam currents and consequent crystal lifetimes are shown in Table 3. The calculations assumed a virtual beam spot of 200μm radius at the collimator. Depending on the flexibility of the beamline optics, one may be able to extend the crystal lifetime by making the beam spot size at the radiator somewhat larger than this. Three different possibilities for the spot size at the radiator are shown in the table. If a mechanism were put in place to raster the crystal across the beam then the spot size would be irrelevant; the only limitation on the duration of an experiment with a single crystal would then be given by the figure in the last column, proportional to the area of the crystal.

6 Beamline considerations

The paper of Kaune *et.al.*[2] offers a thorough description of the SLAC beamline that was used to produce collimated bremsstrahlung for an actual experiment. The intensity spectra at the left, taken at two different orientations of the diamond crystal, were obtained at reduced beam current using a pair spectrometer to measure the photon energy. The narrowness of the peaks and the small incoherent background give proof that very clean monochromatic beams can be obtained in practice with this technique. The yellow shaded curve through the data is my result applying the model described in this report to the SLAC setup. The

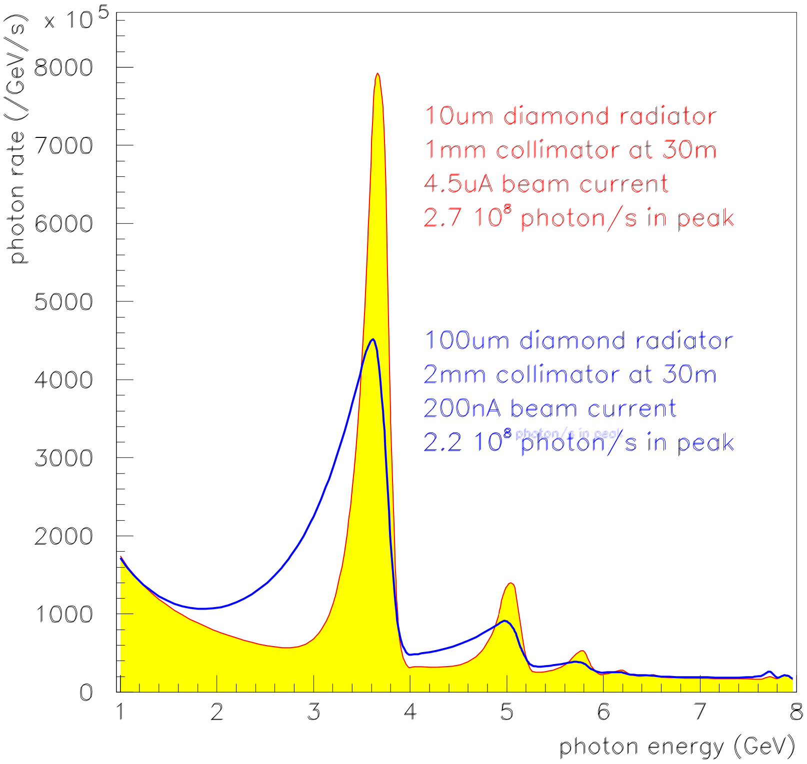

Figure 16: Photon beam spectrum for the conditions of the example experiment described in the text, for two limiting values of the crystal thickness. Note that this plot shows total photon rate rather than ratio of coherent to incoherent flux as before.

Table 3: Lifetime of crystal radiator before it must be moved or replaced in order to prevent degradation of the photon beam from crystal defects.

		beam r.m.s. at radiator			
target thickness	beam current	200μm	500μm	2mm	usable lifetime
100μm	200nA	28h	175h	120d	930 days/cm^2
10μm	4.5μA	1.2h	7.8h	125h	41 days/cm^2

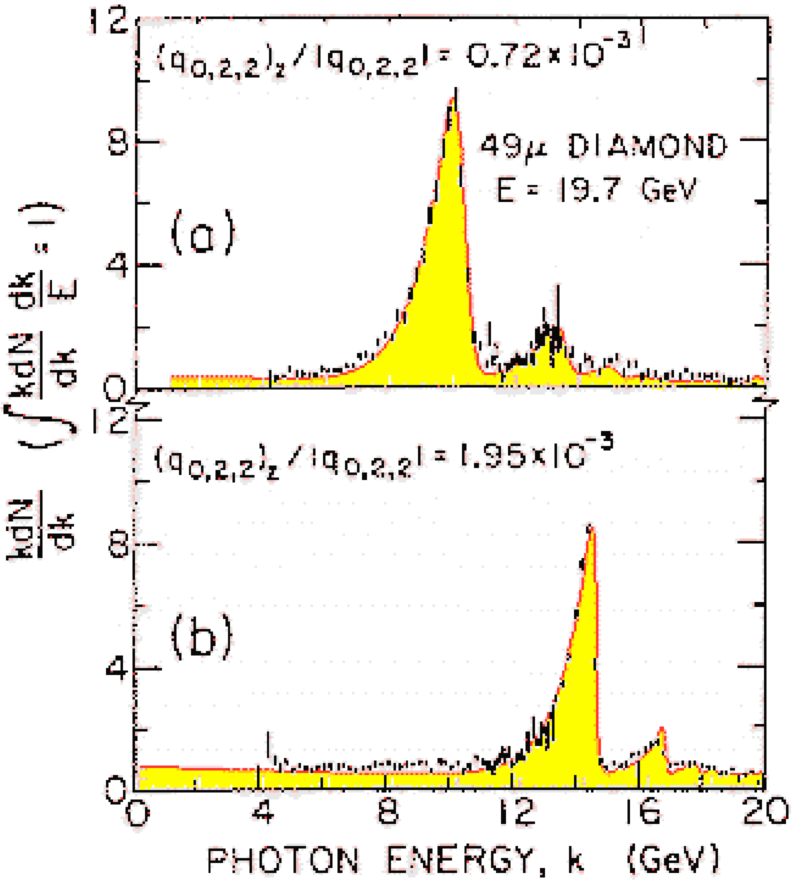

Figure 17: Photon intensity spectrum measured at the coherent bremsstrahlung beamline at SLAC with a pair spectrometer. The data points are taken from Fig. 5 in Kaune *et.al.*[2] and the curves (red with yellow shading) superimposed on the data are calculated within the framework presented in this report.

agreement with the data is excellent, although the vertical scale is not significant (curves are normalized to unity) and the orientation of the crystal was adjusted to put the peaks in the right place. Still, the agreement in peak shape and ratio coherent/incoherent indicates that the essential physical effects have been correctly taken into account.

If beams of comparable quality could be produced at CEBAF, it would provide an attractive alternative to tagged bremsstrahlung for a number of experiments with real photons. The question arises, what are the requirements for a beamline that could deliver such a beam of real photons using electron energies of 8+GeV? In this section I wish to enumerate the key elements in the setup that was used to obtain the excellent results shown above, as a prototype for what might be done at CEBAF. The figure above, taken from the SLAC paper, is set up for 20GeV electrons. The collimator at 91m from the radiator is 2mm in diameter, or 0.42 m_e/E. The beamline elements are discussed below under five headings.

1. crystal mount
   The primary apparatus here is the two-axis goniometer in which the crystal is held and rotated. The goniometer is designed so that it can be pumped down to the vacuum of the beamline. It is powered by high-resolution stepping motors which are remote-controlled by a computer. The step size is 23μr on each axis, which translates for a 20GeV beam and 10GeV photons to increments of 170MeV in the position of the photon peak. In general the step size should be designed to be smaller than or comparable to the mosaic spread of the radiators that it will orient. The mechanical design of the goniometer is simplified by the fact that only a limited range of angles are needed; the SLAC device had a range of $\pm$60mr on each axis. At 8GeV this would limit operation to $x < 0.9$ for the primary coherent peak, which is already beyond the limit where significant coherent enhancements can be obtained.

2. beam optics
   Optimal results for collimated bremsstrahlung require that the electron beam be focused at the position of the collimator to a spot much smaller than the collimator diameter. The SLAC collimator used to produce the above spectra had an inner diameter of 2mm. The calculation which is superimposed upon these spectra assumed a 500μm virtual spot size at the collimator and a beam emittance of 10^{-8}rm, leading to a spot at the radiator of r.m.s. width 2mm. In the paper they give 6mm for the diameter of the beam spot at the radiator, somewhat larger than the f.w.h.m. resulting from my calculation, although the expression "horizontal and vertical size" is not very precise. One side-effect of the large beam spot at the radiator was that it extended the lifetime of the crystal by spreading out the radiation damage over a large surface. The elements responsible for producing the focus are located before the exit from the accelerator, and so are not shown in the above layout. The two magnets which are shown just upstream of the radiator are vertical and horizontal dipoles. They perform the small corrections necessary to keep the photon beam well centered on the collimator. The dipole located between the radiator and the collimator bends the electron beam into the dump.

3. beam controls
   It is very important for the stability of the photon beam that the electron beam focus remain fixed at the center of the collimator; small drifts that would be acceptable for ordinary bremsstrahlung beams produce large distortions in the rate and spectrum of the collimated beam. At SLAC they required that the centroid of the bremsstrahlung photon beam remain within 150μm of the center of the collimator in both horizontal and vertical planes, adding that "During stable operation of the accelerator virtually all of the beam pulses satisfied this criterion." This corresponds to only 6% m_e/E. This exceptional control is accomplished by an active feedback between beam position sensors inside the collimator assembly and the power supplies to the corrector dipoles. The position of the photon beam at the collimator is sensed by a four-quadrant tungsten-pin shower-emission detector located downstream of the first segment (a few radiation lengths) of the primary collimator. The current from these pins is proportional to the local shower intensity. The entire collimator assembly could be remotely rotated through 180 degrees so that the four quadrants could be gain-balanced. The four signals were added and subtracted in two separate circuits to produce horizontal vertical displacement signals. These are

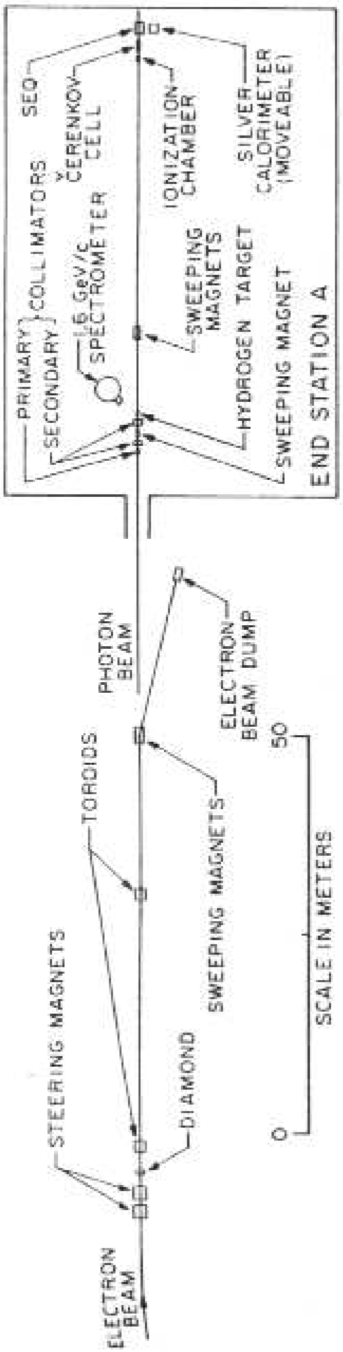

Figure 18: Schematic plan view of the layout of the SLAC experiment. The electron beam dump was actually below the photon beam. The is Fig. 1 from Kaune *et.al.*[2].

read out by the computer for each pulse, and any necessary corrections automatically applied to the corrector power supplies.

4. collimation and shielding
The photon beam collimation consists of a primary collimator, which determines the characteristics of the photon beam, and a set of secondary collimators which help to cut out the secondaries that come from interactions in the primary collimator. The primary collimator at SLAC was 70 radiation lengths of tungsten with a 2mm-diameter-bore. Following this there was a secondary collimator of 6mm-diameter bore made of 30 radiation lengths of copper. There then followed a 0.7 Tm dipole magnet for clearing charged particles out of the beam, and a third collimator of 85 radiation lengths of lead with a diameter of 12mm. The increasing diameters insure that there is no further scraping of the beam formed by the primary collimator. Most of the secondaries arise from showers that leak particles back into the region of the beam, and so they have angular distributions which are much broader than the coherent bremsstrahlung and are blocked by the secondary collimators. The third collimator is necessary in order to catch the charged particles swept from the beam by the dipole.

5. monitoring
The two “toroids” in the above figure are pickup coils which measure the charge in each electron beam pulse. Since the electron beam at SLAC was too large to be entirely contained within the dimensions of the diamond crystal, knowledge of the electron beam current was not sufficient to determine the photon flux. The overall beam intensity was monitored by a total-absorption counter (SEQ in figure), whose was given an absolute calibration was could be checked by comparison with a silver calorimeter, whose response is known. An ionization chamber and a Cerenkov counter also appear in the diagram, presumably to monitor the charged component of the beam. Not shown in the figure is the pair spectrometer used to measure the spectrum of the collimated photon beam. It is not present during ordinary running, as it could only be used with the experimental target removed.

With no online monitor of the photon spectrum, one would have to rely on periodic checks with the pair spectrometer to monitor degradation of the crystal. If it were present, the tagger could provide this function. At reduced beam current the tagger could be run in coincidence with a total absorption counter to measured the photon spectrum instead of having to instrument the focal plane of a pair spectrometer. During normal running, even though the tagger rates might be too high for counting, reading out the current from the tagging counters at reduced voltage would provide a fast online monitor of the status of the crystal and the properties of the coherent photon beam.

7 Summary

1. The process of coherent bremsstrahlung has been well-understood within first-order QED. A simple model involving analytic expressions has been shown to give good agreement with measurements in the regime of interest for photon beams at 8+GeV.

2. With 8GeV electrons it is possible to make coherent bremsstrahlung beams containing pronounced peaks of highly-polarized photons. These peaks can be narrowed by collimation to widths as low as 1-2% r.m.s. The energy and polarization plane of the primary peak can be adjusted by changing the tilt of the crystal radiator. Collimating at 25% m_e/E, the height of the primary peak varies from a factor of 40 at 4GeV to 10 at 6GeV, measured with respect to the intensity of the underlying incoherent bremsstrahlung.

3. Without any collimation at all, an oriented crystal enhances a tagged bremsstrahlung beam by decreasing the relative flux of untagged photons, and producing an appreciable beam polarization over a limited range of photon energies. For experiments not requiring sub-percent photon energy resolution, the use of thin crystals along with collimation can replace tagging as a source of monochromatic

photons. Using this method one can achieve photon fluxes on the order of 10^9/s in the primary peak, with reasonable values for the beam current and crystal lifetime.

4. Intrinsic limitations (multiple scattering, beam emittance, mosaic spread) prevent reduction of the r.m.s. width of the coherent peak below about 2% at 4 GeV, decreasing to 1% at 6GeV, for 8GeV electrons. Further decreases would require the production of thinner crystals than have been obtained so far, and the restrictions on beam current imposed by radiation damage would limit the photon flux that could be reached with them.

5. For absolute measurements the incoherent component of the beam can be removed by subtraction. Running with the crystal tilted far from one of the dominant axes removes the coherent component without affecting the incoherent part, so that the difference reveals the coherent contribution to the data.

6. Implementation requires a *system design* including specialized beamline optics elements, controls, shielding, and instrumentation for monitoring, in addition to the radiator-collimator assembly.

References

[1] D. Zwanziger, "Energy and momentum spectral function of coherent bremsstrahlung radiation," **Phys. Rev. D20** no.8 pp.2001-2026,1979.

[2] W. Kaune, G. Miller, W. Oliver, R.W. Williams, and K.K. Young, "Inclusive cross sections for pion and proton production by photons using collimated coherent bremsstrahlung," **Phys. Rev. D11** no.3 pp.478-494,1975.

[3] H. Bilokon, G. Bologna, F. Celani, B. D'Ettorre Piazzoli, R. Falcioni, G. Mannocchi and P. Picchi, "Coherent bremsstrahlung in crystals as a tool for producing high energy photon beams to be used in photoproducion experiments at CERN SPS," **Nucl. Instr. Meth. 204** pp.299-310,1983.